

Using mathematical morphology to determine left ventricular contours

This article has been downloaded from IOPscience. Please scroll down to see the full text article.

1993 Phys. Med. Biol. 38 1877

(<http://iopscience.iop.org/0031-9155/38/12/012>)

View [the table of contents for this issue](#), or go to the [journal homepage](#) for more

Download details:

IP Address: 158.109.9.220

The article was downloaded on 07/01/2013 at 11:58

Please note that [terms and conditions apply](#).

Using mathematical morphology to determine left ventricular contours

J Pladellorens†, J Serrat‡, A Castell§ and M J Yzuel||

† Departament d'Òptica i Optometria, Universitat Politècnica de Catalunya, Spain

‡ Departament d'Informàtica, Universitat Autònoma de Barcelona, Spain

§ Departament de Medicina Nuclear, Hospital de la Vall d'Hebrò, Barcelona, Spain

|| Departament de Física, Universitat Autònoma de Barcelona, Spain

Received 7 January 1993, in final form 2 August 1993

Abstract. The aim of this study is to investigate the use of mathematical morphology for the determination of left ventricular contours in scintigraphic images using multigated radionuclide angiography. We have developed a completely automatic method that first restores the image with a Wiener filter, then finds the region where the left ventricle is contained, and finally segments the left ventricle contour and a background zone. The contours depend on the values of the parameters that appear in the mathematical morphology method, which are related to the height and the slope of the count distribution. Results obtained with this method are compared with the contours and the background zones outlined by experts on the basis of the number of counts. We study the values of the parameters with which the optimum correlation is obtained.

1. Introduction

Several methods for contour detection of the left ventricle (LV) have been developed for images obtained using equilibrium radionuclide angiography (ERNA) (Chang *et al* 1980) to find wall-motion abnormalities or to measure the volume of the LV. Such measurements, based on the number of counts inside the LV, allow us to calculate the ejection fraction. A linear combination of first and second differences was used to establish an adequate contour (Hawman 1981). Moreover, locating the minimum-cost contour in accordance with the distance or cost function is a common approach to LV segmentation (Reiber *et al* 1983). Duncan (1987) has proposed a knowledge-based strategy joining global and local information in heuristic functions. All these methods are semi-automatic because in order to apply the method an operator should previously determine a rough rectangular region of interest. In this paper we introduce an alternative approach, which is completely automatic, locating the boundary of the LV in the left anterior oblique (LAO) view, based on mathematical morphology operations.

Mathematical morphology has been successfully used before in medical image analysis. For instance, it has been used to extract the rachidian canal from CT images, or mammalian nodules and brain tumours from NMR images (Bartoo *et al* 1988). Furthermore, mathematical morphology techniques have proved useful in brain lesion analysis related to Alzheimer's disease (Schmitt and Preteux 1986).

Before using mathematical morphology, we apply a Wiener filter, not only because of its noise-removal property but also because it restores the image by sharpening the contours. This filter has been used by several researchers to improve scintigraphic image quality (King

et al 1983, Miller et al 1984, Hon et al 1989). The method is applied to 25 studies and the results are compared with the contours outlined by three experienced operators.

In section 2 we will describe the procedure for obtaining the LV contour and the background, and the steps needed to obtain the net counts inside the ventricle, which are related to its volume. In section 3 we give the results obtained with the automatic method and a comparison with the results of experts.

2. Methods

Before attempting to extract the LVs of a sequence of images, we apply a Wiener filter to remove the noise and restore the sequence of images. The next step is the partition of each filtered image into different regions. One of these regions will contain the whole LV. After identification, we proceed to delimit the exact contour inside the region by means of a sequence of morphological operations. Also, using mathematical morphology we automatically find a background zone found by most experts manually. Hence, we shall review the bases of mathematical morphology and especially the operations involved in our process. We also present one particular problem in identifying the LV region and the way it is solved.

2.1. Preprocessing

Scintigraphic images are characterized by having a low signal-to-noise ratio inherent to their process of emission and capture of photons. In the past, several methods of smoothing in scintigraphic images were tested, the median filter being a suitable approach that maintains the contours (Deconink and Luypaert 1982, Grochulski et al 1985). Nevertheless, it does not eliminate enough noise to obtain images in which mathematical morphology can be applied. Here we use the Wiener filter, which uses as its optimality criterion the minimization of the mean square error between the undistorted image of the object and the filtered image. Its frequency-domain form is (Pratt 1991)

$$H'(u, v) = [1/H(u, v)]|H(u, v)|^2/[|H(u, v)|^2 + S_n(u, v)/S_f(u, v)] \quad (1)$$

where

$$|H(u, v)|^2 = H^*(u, v)H(u, v). \quad (2)$$

$H(u, v)$ is the system transfer function, $H^*(u, v)$ is its conjugate, S_n is the noise power spectrum, S_f is the object power spectrum, and u and v are the frequency variables.

However, it is necessary to know the point spread function (PSF) of the gamma camera and also the power spectrum of noise and object. In order to determine the PSF, we have assumed that it can be approximated by a Gaussian function with standard deviation $\sigma = \text{FWHM}/2.35$ (Barret and Swindell 1982), where FWHM is the full width at half maximum, obtained experimentally with the same gamma camera by picturing a point source with the necessary correction (Puchal 1988). We also assume the PSF to be invariant with position and depth.

In order to obtain the object and noise power spectra, if we assume a Poisson noise distribution we may use the results of Goodman and Belsher (1976)

$$S_g(u, v) = [S_g(u, v) - S_n]/H(u, v)^2 \quad (3)$$

S_g being the degraded image power spectrum and S_n the noise power spectrum, which is constant and equal to the average of counts per pixel. In figure 1 we can see an example of restoration by this filter.

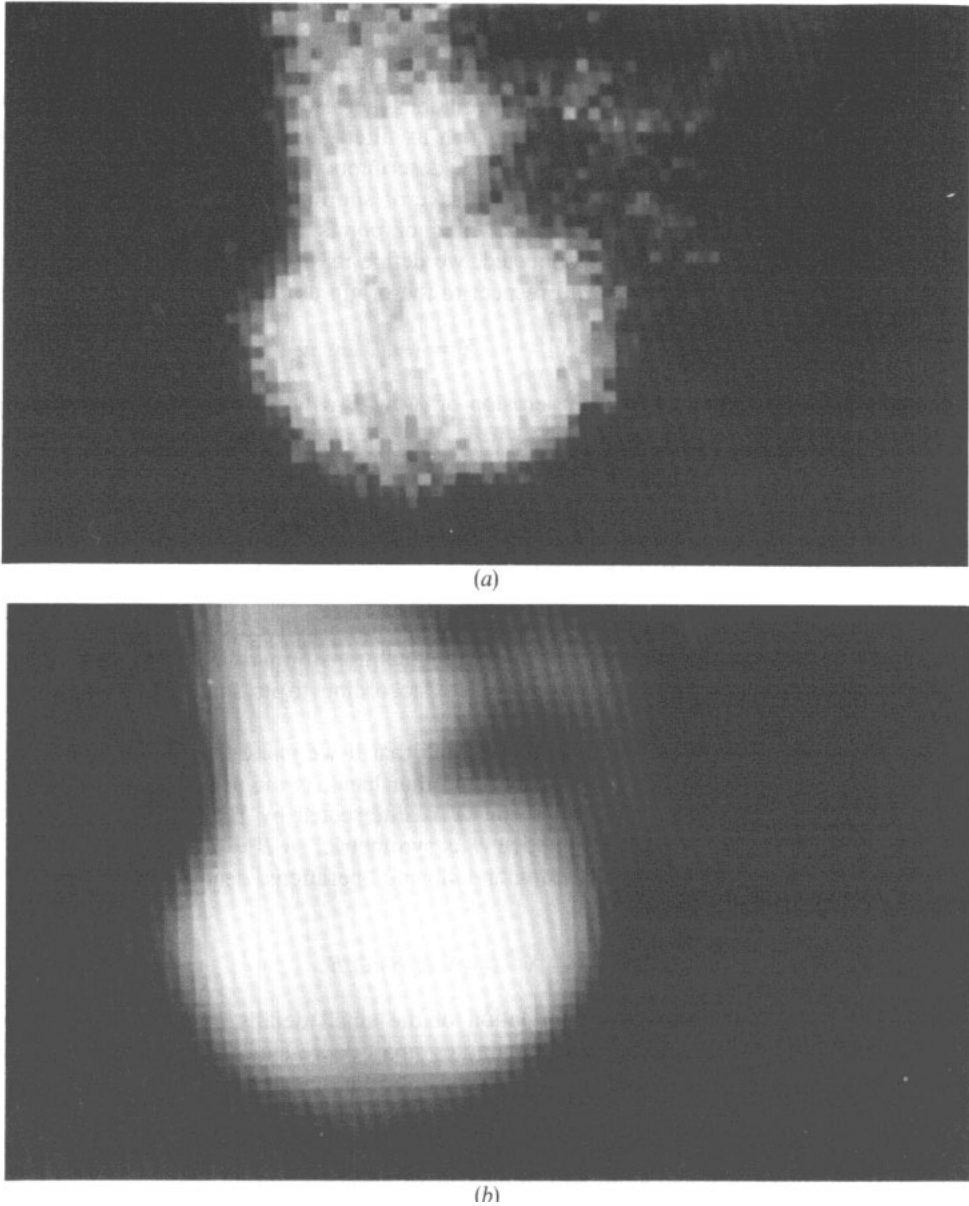


Figure 1. LV image in diastole: (a) original image; (b) preprocessed image after applying the Wiener filter.

2.2. Mathematical morphology

There are different general frames from which to treat the problem of image processing and analysis. One of the best known is that based on signal theory in which the image is considered to be the result of sampling and quantizing a two-dimensional signal. However, in mathematical morphology (Stenberg 1986, Serra 1986), both binary and grey-scale images are seen as one or more sets of points. All operations are based on the geometrical

relationship between the different points of such sets. As Serra (1986) has pointed out, mathematical morphology is the application of the lattice theory to spatial structures. More complex and powerful operations are built from set union, intersection, difference, and complementation, and two basic transformations—erosion and dilation. We obtain algorithms of great utility in image analysis such as filters, granulometries, segmentation algorithms, texture analysis parameters, and shape descriptors. Next, we shall consider some of the basic morphological operations. For the sake of simplification, we shall consider a binary image in a discrete space. Given a set X of points belonging to the set E that contains all the points not specially connected, we define its translation X_h according to a vector h , and the symmetric set \check{X} with respect to the origin as

$$X_h = \{x \in E, x - h \in X\} \quad \check{X} = \{-x, x \in X\}. \tag{4}$$

Given two sets X and B , we define the erosion of X by B as

$$X \ominus \check{B} = \{x, B_x \subset X\} \tag{5}$$

and the dilation of X by B as

$$X \oplus \check{B} = \{x, B_x \cap X \neq \emptyset\}. \tag{6}$$

B is a special set, called a structuring element, which has a defined centre or origin. The structuring element acts as a parameter of morphological transformations and the results and operations obtained show considerable differences according to its shape, size and centre position.

Erosion is the set of points belonging to X such that if we make the B centre coincide with them, B is included in X . Dilation, on the other hand, is the set of points such that if we make the B centre coincide with them, X is intersected by B . In figure 2 we see examples of dilation and erosion. In practice B is symmetric, so $B = \check{B}$.

The next level is formed by the opening and closing operations, denoted by X_B and X^B respectively, and defined as

$$X_B = (X \ominus \check{B}) \oplus B \quad X^B = (X \oplus \check{B}) \ominus B. \tag{7}$$

The effects of the opening are the elimination of the small details of X , separating the weakly joined components. The closing eliminates small depressions and joins the nearest components. It should be noted that in general morphological transformations are not reversible.

Finally, we shall describe three more operations: hit-or-miss transform, thinning, and thickening used in the segmentation algorithm that we shall use.

The hit-or-miss transform is defined as

$$X \otimes T = (X \ominus \check{T}^1) \setminus (X \oplus \check{T}^2) \tag{8}$$

where the structuring element $T = \{T^1, T^2\}$ is composed of two disjunctive parts with a common centre. This transform returns the pixels whose local neighbourhood configuration coincides with that specified through T^1 and T^2 : T^1 indicates which pixels must be unity and T^2 which ones must be zero. For instance, the following T^1 and T^2 :

$$T^1 = \begin{matrix} \cdot & \cdot & \cdot \\ \cdot & \cdot & \cdot \\ 1 & 1 & 1 \end{matrix} \quad T^2 = \begin{matrix} 1 & 1 & 1 \\ \cdot & 1 & \cdot \\ \cdot & \cdot & \cdot \end{matrix}$$

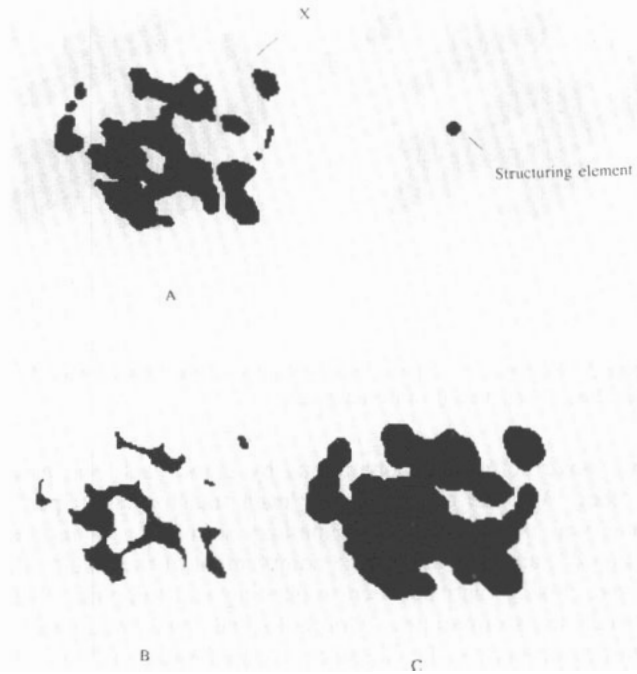


Figure 2. Examples of erosion and dilation of a binary image X by a structuring element B : (a) original binary image; (b) erosion of (a); (c) dilation of (a).

make the hit-or-miss return the pixels whose local configuration is equal to the following T :

$$T = \begin{matrix} 0 & 0 & 0 \\ \cdot & 0 & \cdot \\ 1 & 1 & 1 \end{matrix}$$

where \cdot means that both 0 and 1 are accepted.

Now, the thinning $X \circ T$ and thickening $X \odot T$ of X by one of these biphasic structuring elements T are the set difference and the set union with its hit-or-miss transform respectively:

$$X \circ T = X \setminus (X \otimes T) \quad X \odot T = X \cup (X \otimes T) \tag{9}$$

where $X \setminus Y = X \cap Y^c$, and Y^c is the complementary set with respect to the universal set E .

In figure 3 we see examples of thinning and thickening. Thickening and thinning operations are not usually applied in a single direction of the structuring element, but T is rotated to obtain the same thinning or thickening in all directions.

We shall name the structuring element sequence obtained by successive rotations of T $\{T\} = T_1, T_2, \dots, T_n$. Then one thickening in all directions is denoted by

$$X \odot \{T_i\} = \{ \dots [(X \odot T_1) \odot T_2] \dots \} \odot T_n \tag{10}$$

where n is the number of possible rotations without repeating the initial T .

Finally, we denote the transformation of X by T conditional to a set Y as

$$T(X); Y = T(X) \cap Y. \tag{11}$$



Figure 3. Examples of thinning and thickening of the binary image X : (a) thinning of the image $2(a)$; (b) thickening of the image $2(a)$.

As we can see, we have defined the operations by pairs, each one being in some way opposite to each other. We can check that for each transformation performed on X , its pair acts in the same way on X^C , the complementary set of X . For instance, eroding X is equivalent to dilating X^C , and then taking the complement of the result. The same happens between opening and closing, and between thickening and thinning. This relationship is called duality between transformations. Morphological transformations can be classified according to a series of properties. For instance, a transformation T is

- (i) antiextensive if $T(X) \subset X$,
- (ii) idempotent if $T[T(X)] = T(X)$, and
- (iii) homotopic if it keeps the homotopic tree, that is, the number of holes and regions and the hierarchical inclusion relationship between them.

Erosion, opening and thinning are antiextensive. Thinning and thickening may become homotopic by selecting the appropriate structuring element. This property is especially important for the thickening used in the region of influence of the local-maxima algorithm of section 2.3. Neither of them is idempotent, but if we define the infinite sequence $\{T_j\} = T_1, T_2, \dots, T_n, T_1, \dots, T_n, \dots$ then $X \odot \{T_j\}$ is idempotent.

The operations we have seen through binary images can be easily extended to grey-scale images if we express them as sets. We consider an image to be a function $f(x, y)$ on the plane. Hence, we can express it as a set $U(f)$, called the umbra and defined as

$$U(f) = \{(x, y, z) : z \leq f(x, y)\}. \quad (12)$$

Henceforth, we shall denote $U(f)$ as f in any morphological operation. Erosion and dilation operations become

$$(f \ominus B)(a) = \inf[f(b), b \in \check{B}_a] \quad (f \oplus B)(a) = \sup[f(b), b \in \check{B}_a] \quad (13)$$

where a and b are points and B is a set of a three dimensional space. If B is flat, i.e. $B(i, j)$ is only zero or unity, erosion and dilation are simply the local minimum and maximum respectively.

2.3. Segmentation of the left ventricle

In order to explain the segmentation algorithm, we consider a grey-scale image as a topographic surface or relief. The local maxima correspond to summits and the minima

to troughs. We want to associate these points with their regions of influence, which will be hills in maxima and watersheds in minima. We shall see that segmentation by regions of influence of maxima allows to delineate the LV in filtered scintigraphic images.

Let us suppose that it is raining on our topographic relief. When the water reaches the surface it runs down the highest-slope path until it reaches a minimum or sink, where it stops. The watershed associated with a local minimum is the set of points from which the path with the highest slope reaches the nearest local minimum. The set of points from which several paths of maximum slope to different sinks arise is called a divide. Because of the duality, the regions of influence of the local maxima of $-f$ are the watersheds of f .

From this topographical viewpoint, in our filtered images in LAO view the LV appears as a gentle hill with a maximum of grey level (figure 4). It is separated by a saddle and two elevated valleys from other mountains corresponding to other cardiac cavities, which are full of blood. The proximity of these two structures and their weak separation constitute the main obstacle to segmenting the LV. Nevertheless, image segmentation in regions of local maxima influence will separate both structures optimally.

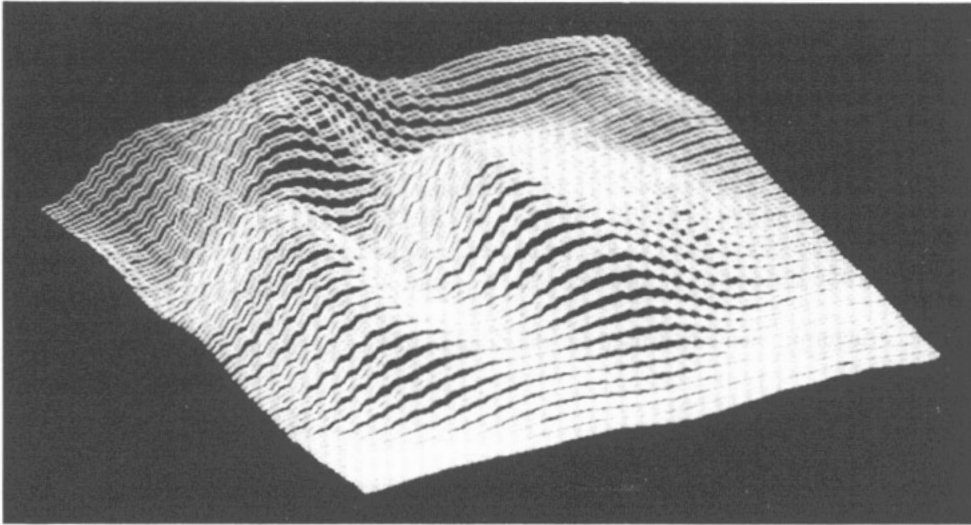


Figure 4. A filtered image seen as a topographic relief where the grey level of each pixel is converted into height.

Moreover, the whole ventricle is included inside the region of influence of its maximum. The process of segmentation follows three steps: (i) calculation of the regions of influence of local maxima; (ii) selection of the region corresponding to the LV; and (iii) extraction inside this region of the LV contour.

(i) Calculation of the regions of influence of local maxima. We have implemented a parallel algorithm in order to obtain such regions, which are able to process all the images of a sequence at the same time.

We define the different image levels of image f as $X_i = \{p : f(p) \geq i\}$ for $i = 0, 1, \dots, n$, where n is the maximum grey-level value. Our algorithm processes each level of the image from X_n to X_0 . At each level X_{n-i} , we carry out a homotopic thickening of the partial result Y_{i-1} obtained to date, conditional to X_{n-i} . To the result we add Z_i , the maxima that appear just at the current level. So, the algorithm is

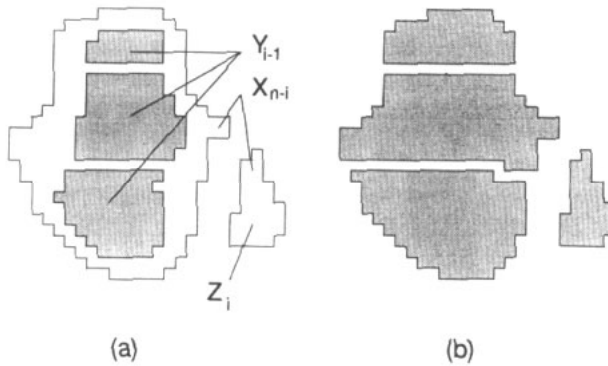


Figure 5. A step of the region of influence of the local maxima algorithm: (a) Y_{i-1} ; (b) Y_i .

$$Y_0 := X_n$$

for $i := 1$ to n

$$Z_i : X_{n-i} \setminus (Y_{i-1} \oplus \{B\}; X_{n-i}) \quad Y_i := (Y_{i-1} \odot \{T\}; X_{n-i}) \cup Z_i. \quad (14)$$

In practice it is not necessary to perform thickening or dilation by an infinite sequence of structuring elements $\{T\}$ and $\{B\}$. By $(Y_{i-1} \oplus \{B\}; X_{n-i})$ and $(Y_{i-1} \odot \{T\}; X_i)$ we only mean that is necessary to achieve the idempotence of these operations on the current image. Considering the difference of size between Y_{i-1} and X_{n-i} , sequences of 20 elements are sufficient.

The structuring element B used for the dilation in $Y_{i-1} \oplus \{B\}$ is

$$B = \begin{matrix} 1 & 1 & 1 \\ 1 & 1 & 1 \\ 1 & 1 & 1 \end{matrix}$$

For images on a hexagonal grid it is possible to perform a homotopic thickening with a unique structuring element T . However, in the square grid, as in our case, it is necessary to successively use the four rotations of the following structuring elements P and Q (Coster and Chermant 1989):

$$P = \begin{matrix} 1 & 1 & 1 \\ \cdot & 0 & \cdot \\ 0 & 0 & 0 \end{matrix} \quad Q = \begin{matrix} \cdot & 1 & 1 \\ 0 & 0 & 1 \\ \cdot & 0 & \cdot \end{matrix}$$

One thickening by all different rotations of $\{P\}$ of P expands in one pixel the vertical and horizontal borders of X and the thickening by $\{Q\}$ expands its corners, that is the L-shaped parts of its border. The thickening example of figure 3 has been computed in this way, applying the rotation sequence of P and Q several times in succession. The example of thinning used their complement.

Hence, the last expression of the algorithm (14) becomes

$$Y_i := \left[\dots \{[(Y_{i-1} \odot \{P\}) \odot \{Q\} \odot \{P\}] \odot \{Q\}\} \dots; X_{n-i} \right] \cup Z_i. \quad (15)$$

Finally, Y_n is a binary image that contains the zones of influence of the maxima at unity and the border between them at zero. In figure 5 we can see a step of this process in a scintigraphic image, and in figure 6 the last result Y_n , inverted and added to the image.

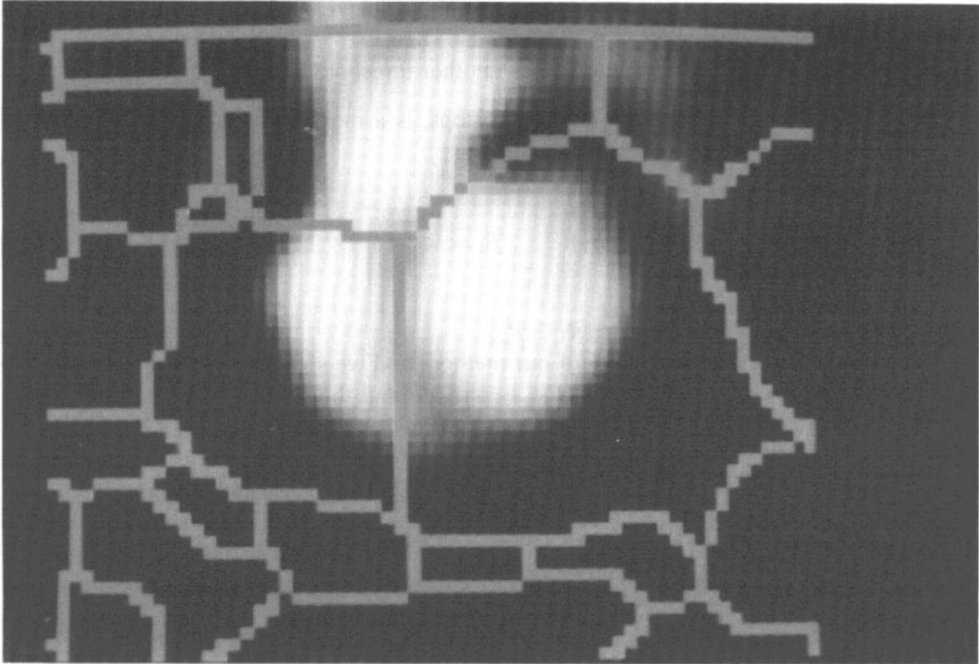


Figure 6. Image partition in maxima regions of influence.

The property of thickening to maintain homotopy and the fact that it is conditioned at the next level causes the different regions of influence not to overlap.

(ii) Selection of the regions of influence of the LV. In order to identify the region that contains the LV, we shall make the assumption that this region will show an elevated maximum and that its position is at the bottom right with respect to the centre of mass of the image.

Considering the grey level at each point (i, j) , the centre of mass (x_g, y_g) of f is calculated as

$$x_g = \frac{1}{N^2} \sum_{i=1}^N \sum_{j=1}^N i * f(i, j) \quad y_g = \frac{1}{N^2} \sum_{i=1}^N \sum_{j=1}^N j * f(i, j) \quad (16)$$

where N refers to the number of lines and columns.

In the image, two zones with high grey level appear. One corresponds to the LV and the other to the right ventricle (RV) plus cavities joined in the same position due to the angle of capture. The centre of mass is located between these two zones.

The local maxima are calculated as the points of the image that are invariant with dilation. We eliminate the points whose intensity does not exceed half of the maximum grey level and from the rest we choose as a part of the summit of the LV the points located to the right of the centre of mass at the bottom.

(iii) Extraction of the left ventricular contour. As we see in figure 6, not all of the region of influence belongs to the LV. We have to choose the part whose mountain slope is marked, and also the parts with a lower but elevated slope, i.e., with high intensity.

Hence, we shall take as points of the LV those having:

- a grey level higher than a certain threshold value t_1 , which is sufficiently high to select only LV points (region R_1); and
- a gradient magnitude that overcomes another threshold value t_2 (region R_2).

The gradient, like all other segmentation steps, is a morphological operation. Given a continuous function f , we define the gradient as

$$\text{grad} f = f - (f \ominus B_1) \quad B_1 = \begin{matrix} \cdot & \cdot & \cdot \\ 1 & 1 & 1 \\ \cdot & \cdot & \cdot \end{matrix}$$

so the region of the LV will be $R = R_1 \cup R_2$.

t_1 and t_2 are the only parameters of our method, and we shall use them to minimize the difference between the results that t_1 and t_2 provide and the results given by radiologists. Once we have joined the two resulting sets of points, we have a region R that often has an irregular contour, or small pores of few pixels. In order to eliminate these features, we apply a closing operation followed by an opening. The first fills the holes and the second eliminates the small protrusions. The closing structuring element must be small enough to preserve the shape of the segmented region (an excessive smoothing would distort it, making the final shape similar to the structuring element) but at the same time it must be able to fill the possible pores. We chose a structuring element C

$$C = \begin{matrix} \cdot & \cdot & \cdot & 1 & \cdot & \cdot & \cdot \\ \cdot & \cdot & 1 & 1 & 1 & \cdot & \cdot \\ \cdot & 1 & 1 & 1 & 1 & 1 & \cdot \\ 1 & 1 & 1 & 1 & 1 & 1 & 1 \\ \cdot & 1 & 1 & 1 & 1 & 1 & \cdot \\ \cdot & \cdot & 1 & 1 & 1 & \cdot & \cdot \\ \cdot & \cdot & \cdot & 1 & \cdot & \cdot & \cdot \end{matrix}$$

The opening, however, must be performed by a smaller structuring element in order to preserve ventricle regions smaller than C , a frequent situation in some patients in systole. Hence the opening uses a structuring element D

$$D = \begin{matrix} 1 & 1 & 1 \\ 1 & 1 & 1 \\ 1 & 1 & 1 \end{matrix}$$

2.3.1. A special case. There is a situation that can arise in certain sequences and which needs additional treatment: the absence of any maximum associated with the LV.

Sometimes, the systole frame and those closest to it may not have a local maximum for the LV. This is due to the fact that the ventricle appears not as a separate mountain, but as a reinforcement of the RV.

Possible causes are an unfavourable angle of vision, or the fact that the ventricle has a very low volume. Obviously, without a maximum we shall not have a region of influence that contains the ventricle and we shall not be able to continue.

To solve the problem, we shall make the assumption that the LV region of influence does not differ much from one frame to the next. This allows us to take the influence zone of the nearest frame with a maximum. Once this is done, the process proceeds as usual.

2.4. Background determination

Once we have outlined the left ventricular contour, we determine a background zone by dilating the contour. We wish to find a background zone similar to that found by experts. So we try to introduce in our automatic method the information we obtain from the experts, let us say the distance from the contour and the angle with respect to the horizontal where most experts fix the background zone. So we dilate the left ventricular contour using the structuring element D , n times, and subtract from it the image obtained by dilating the contour $n - k$ times, using the same structuring element.

We obtain one ring, then we consider a part of this ring in the bottom right part of the image in a similar way as most experts do.

2.5. Hardware and software

The algorithm corresponding to image segmentation described in this paper was implemented in a VIX system for image processing (Unix version of Vicom/Vdp), which is able to perform a set of basic morphological operations in parallel over all the points of an image. Therefore, by putting the whole sequence in a 256×512 pixel image, we can perform most of the process (extraction of local maxima zones of influence and of regions R_1 , R_2 and R) simultaneously.

The rest of the program was written in Pascal in a Microvax of 10 Mb with central memory connected to the VIX by Ethernet.

3. Results

3.1. Preliminary results

The segmentation lines were obtained in 25 sequences. Only in two sequences was there an incorrect segmentation due to the low quality of images. In the selection step of zones belonging to the LV the algorithm never failed.

The contour detection results inside the selected zone were strongly dependent on the structuring element B used to determine the gradient. We studied the effect of applying different structuring elements. The use of a non-symmetrical element does not give good results. This is because it enhances the main direction of the element, and this direction does not always coincide with that of the highest gradient in the ventricle image.

We studied the effect of varying the values of t_1 (grey-level threshold) and t_2 (gradient threshold). If t_1 is too low one obtains a ventricle that is too big; if it is too high the program gives a zone for the ventricle area that is too small.

Likewise, the election of a t_2 that is too low gives a large number of points, which gives as the final result an LV that is too big.

3.2. Measurement of the left ventricle by experts

To test our results we compared them with the results obtained by three experts who routinely outlined the contours by hand in the hospital. We asked them to outline the left ventricular contour in diastole and systole and a background zone in the 25 cases. The results they obtained were compared on the basis of the number of counts inside the contours. Their results were rather similar. Comparison between experts 1 and 2 gives a regression line (expert 2) = 0.93 (expert 1) - 4254, and a correlation coefficient $r = 0.96$; comparison between experts 2 and 3 gives a regression line (expert 3) = 1.00 (expert 2) + 2255, and a

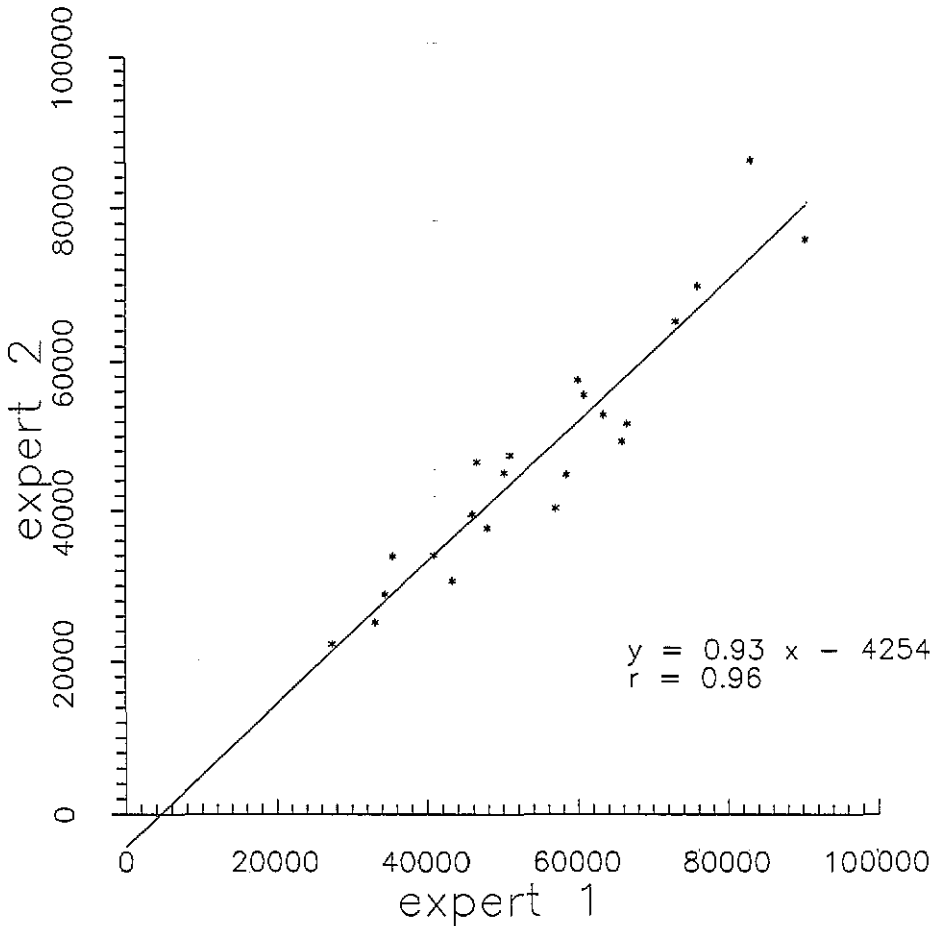


Figure 7. Comparison of the counts inside the contour found by the experts in 23 cases: comparison of the results between two experts in diastole. r is the correlation coefficient.

correlation coefficient $r = 0.96$; and comparison between experts 1 and 3 gives a regression line (expert 3) = 0.98 (expert 1) + 715. In figure 7 we show the comparison between the results obtained by two experts.

To find the best parameters t_1 and t_2 of our method, we minimize the difference between the results of our method and the average of those of the experts in diastole according to the formula

$$\text{dif} = \sqrt{\sum_{i=1}^N (C_{\text{exp}_i} - C_{\text{mor}_i})^2} \quad (17)$$

where dif is the difference between the experts and the automatic method, C_{exp_i} is the average of the total counts inside the contours outlined by experts, C_{mor_i} is the total counts inside the contour found by the automatic method, and N is the number of cases.

Figure 8 shows the relation between the difference (dif) and the value of t_1 keeping t_2 constant. In diastole, t_1 (grey level) and t_2 (gradient level) were optimized by least-squares differences and we obtained the result that the difference is minimized for $t_1 = 75$ and

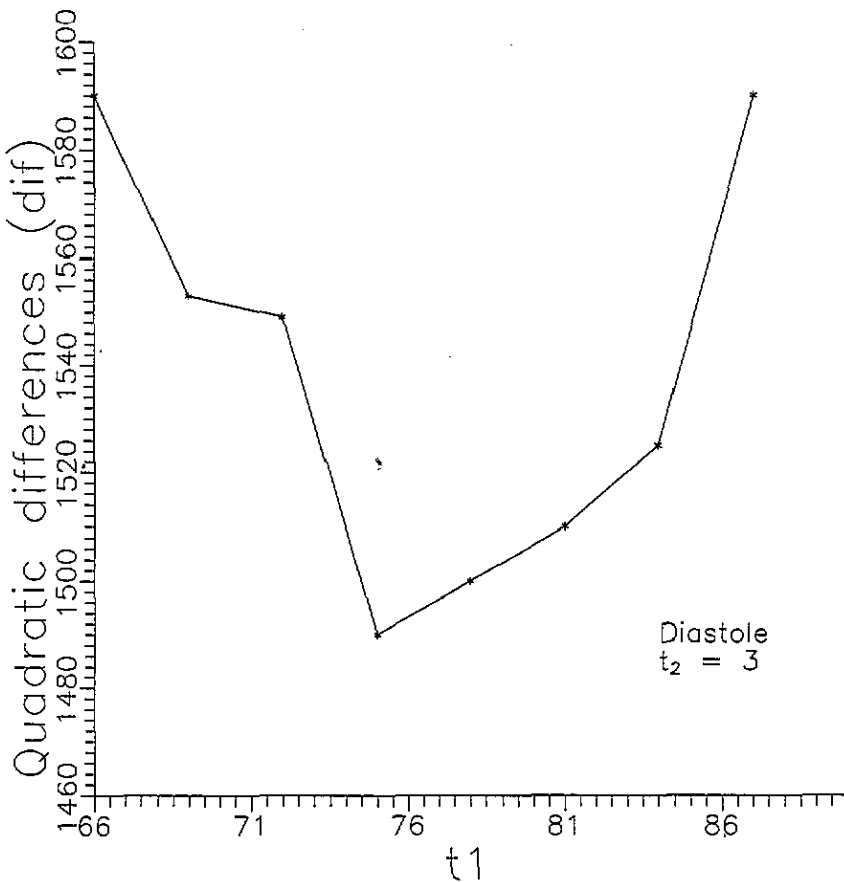


Figure 8. Relation between the difference of the results of our method from the average of those of the experts in diastole and the value (t_1) of the grey-level threshold, the gradient threshold (t_2) being constant ($t_2 = 3$).

$t_2 = 3$. We repeated the same study for the images in systole and obtained the result that the difference is also minimized in this case for $t_1 = 75$ and $t_2 = 3$.

With these values of t_1 and t_2 , in figure 9 we compare the results found by this method with the average of the results found by experts. The regression line is similar to $y = x$, and the correlation coefficient is 0.91 in diastole and systole.

To determine the background we consider the contours found for the values $t_1 = 75$ and $t_2 = 3$. A background zone is determined using the contours found for the values $t_1 = 75$ and $t_2 = 3$ with $n = 3$ and $k = 2$ and an arc of 30° (section 2.4). We consider as the centre of the circle the centre of mass of the LV, then we calculate the values of the background by averaging the counts per pixel in the background zone, determined as explained in section 2.4. Once this background value is evaluated for an image we can obtain the net counts, which are directly related to the volume of the LV. We use the following formula:

$$NC = TC - B * S \tag{18}$$

where NC is the net counts, S the area of the contour, TC is the total counts, and B the background per pixel.

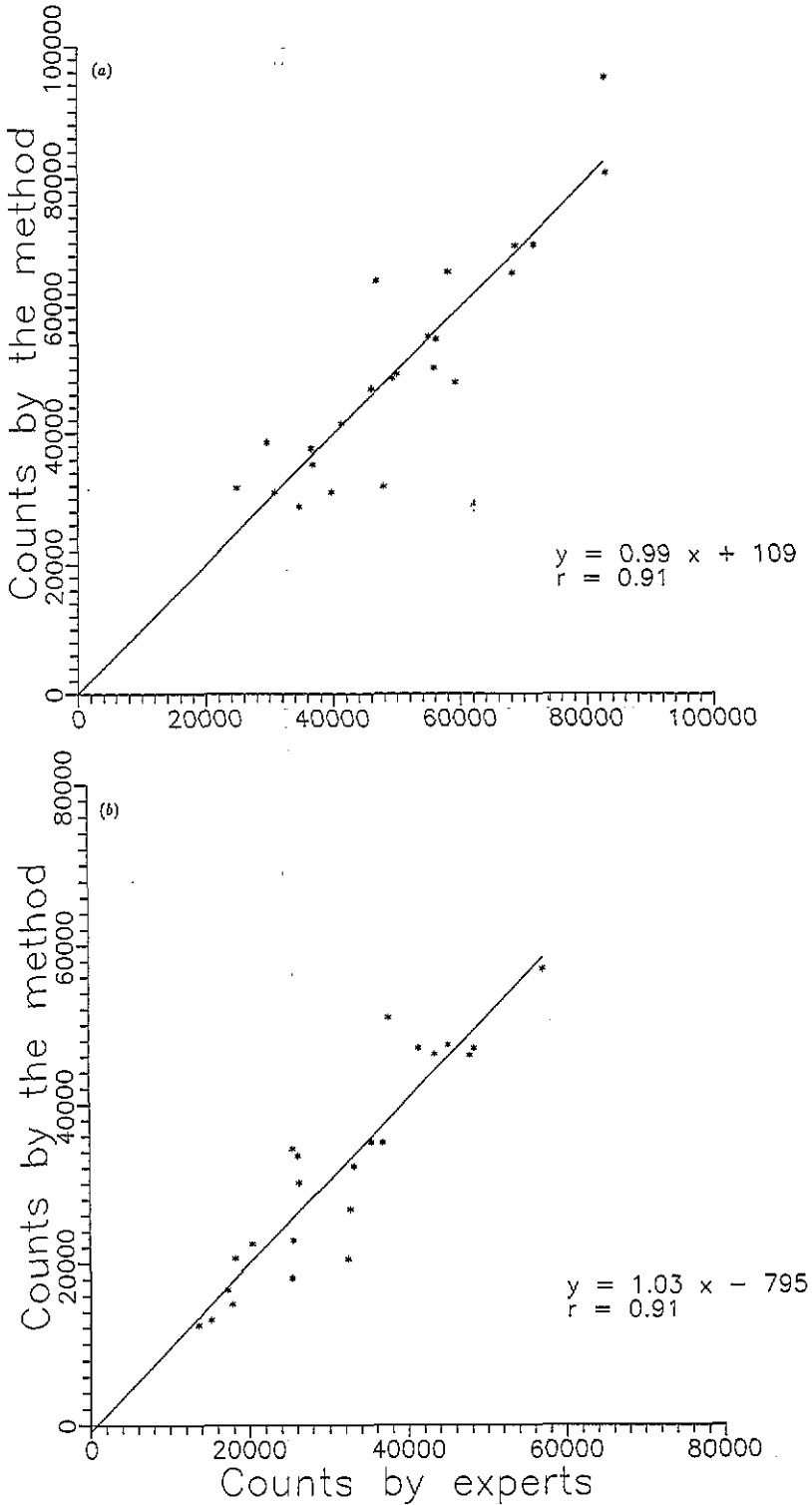


Figure 9. Comparison of the results found by this method with the average of the results found by experts. r is the correlation coefficient. (a) in diastole; (b) in systole.

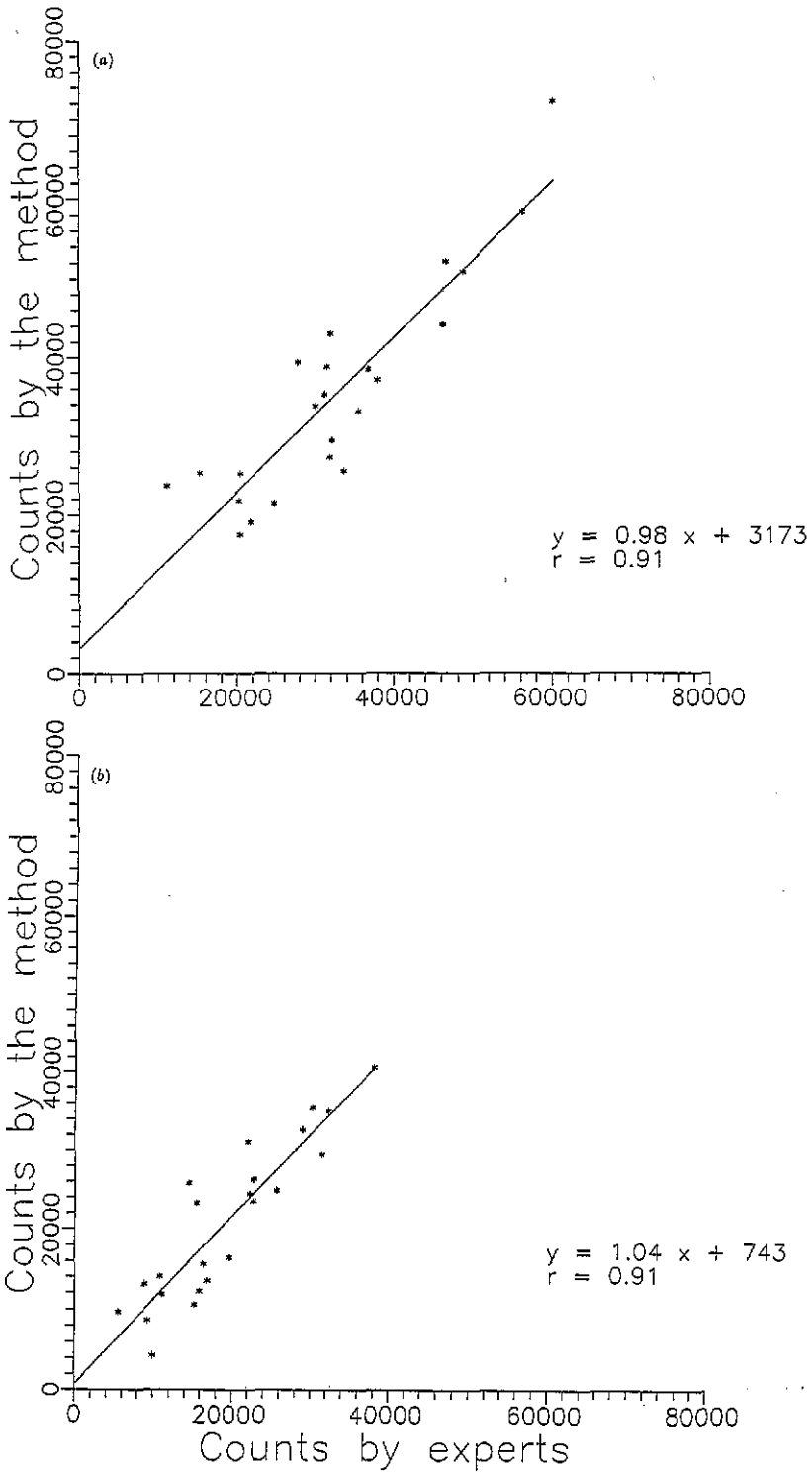


Figure 10. Comparison of the results found by this method with the average of the results found by the experts, when we consider the net counts inside the LV. r is the correlation coefficient. (a) in diastole; (b) in systole.

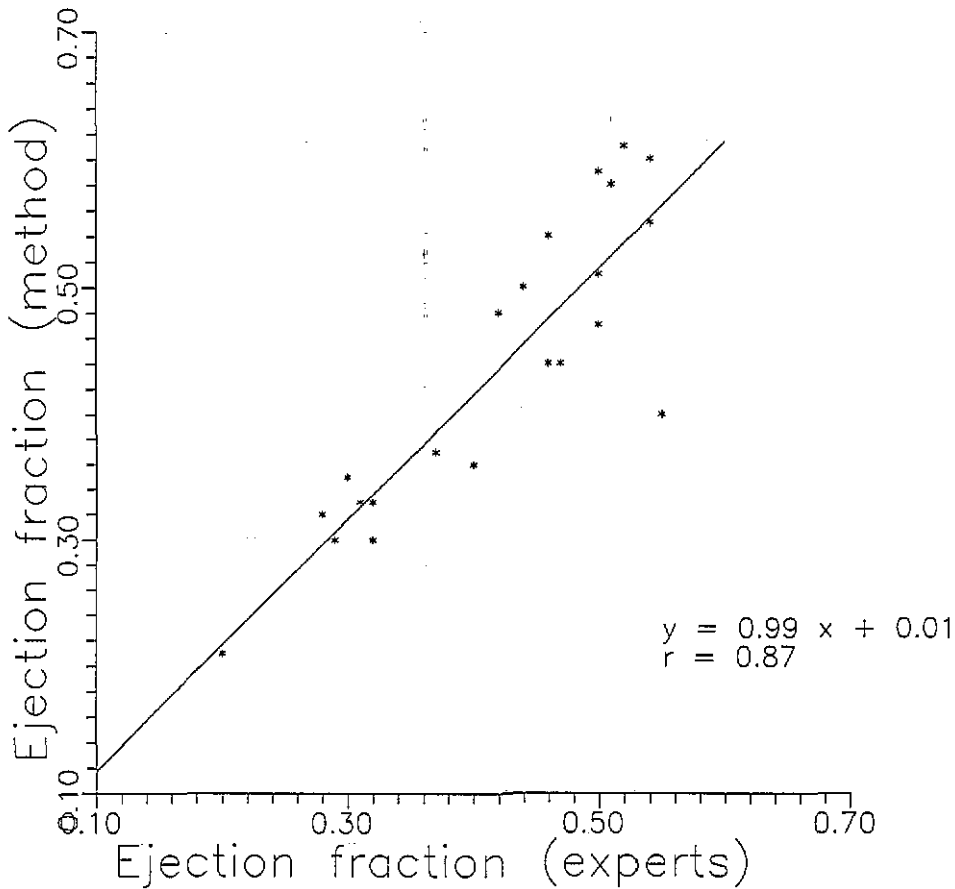


Figure 11. Comparison of the ejection fractions found by this method with the ejection fractions found by the experts. r is the correlation coefficient.

With the values of background per pixel determined as described previously, we calculated the net counts of the ventricle in diastole and in systole. We also calculated the net counts of the ventricle in diastole and systole using the total counts and the background per pixel found by experts.

In figure 10 we compare these results, which have regression lines close to $y = x$ and correlation coefficients of 0.90 in both cases.

We also study the values of ejection fraction EF defined by

$$EF = (V_D - V_S) / V_D \quad (19)$$

where V_D and V_S are the volumes of the left ventricle in diastole and systole respectively. Once we have calculated the net counts in diastole and systole the volumes are calculated by multiplying these net counts by a constant. So the ejection fraction is given by

$$EF = (NC_D - NC_S) / NC_D \quad (20)$$

where NC_D is the number of net counts in diastole and NC_S the number of net counts in systole.

In figure 11 we compare the ejection fractions, obtaining a regression line close to $y = x$ and a correlation coefficient of 0.87.

4. Discussion

We investigated the utility of mathematical morphology for the determination of left ventricular contours in scintigraphic images using multigated radionuclide angiography. This is a completely automatic method, which assures total reproducibility since no operator is needed. The method is carried out in two stages: (i) the rough outline of the LV region within the whole image; and (ii) the accurate outline of the ventricle within the rough outline defined in stage (i). The method in both stages is based on mathematical morphology. A preliminary restoration of the image is needed for the application of mathematical morphology. The original images were studied by three experts who manually outlined the contours of the LV. Taking as a basis the number of counts inside the contours we compared the results, which gave good coincidence with a correlation higher than 0.94. We obtained the mean value of the results of the experts and then we adjusted our method by changing the values of the two parameters t_1 and t_2 .

We found that the best approximation was given with $t_1 = 75$ and $t_2 = 3$, in both diastole and systole. In a similar way, taking the contour as a basis we can find a region in which the value of the background is equal to that determined on average by experts. Finally we calculated the net counts inside the contour and then compared this with the average net counts determined by experts, obtaining a good correlation. We also obtained good correlation between the ejection fractions, although the correlation coefficient was lower than that found between experts. We suppose that this is because the experts have a common background knowledge of the problem, so it is understandable that they coincide with each other more than the method coincides with the mean value of experts.

In conclusion, the method permits an automatic determination of the left ventricular contour and a background zone in similar way to that used by experts.

Acknowledgments

We should like to thank Dr S Aguadé and Dr M Fraile for their collaboration as experts in this work.

We should like to thank the CIRIT (Commissió Interdepartamental per la Recerca i la Innovació Tecnològica de la Generalitat de Catalunya) (AR88), for the financial help provided for this work.

References

- Barret H H and Swindell W 1982 *Radiological Imaging* vol 1 (New York: Academic) p 273
- Bartoo G T, Kim Y, Haralick R M, Noehlin D and Sumi S M 1988 Mathematical morphology techniques for image processing applications in biomedical imaging *Proc. SPIE* **914** 466-75
- Chang W, Henkin R, Hale D and Hall D 1980 Methods for detection of left ventricular edges *Sem. Nucl. Med.* **10** 39-53
- Coster M and Chermant J L 1989 *Precis d'Analyse d'Images* (Paris: CNRS) (in French)
- Deconink F and Luybaert R 1982 Design and evaluation of median filters for scintigraphic image filtering *Proc. ISMII '82* pp 20-3

- Duncan J S 1987 Knowledge directed left ventricular boundary detection in equilibrium radionuclide angiography *IEEE Trans. Med. Imaging* **MI-6** 326-37
- Goodman J W and Belsher J F 1976 Fundamental limitations in linear invariant restoration of atmospherically degraded images *Proc. SPIE* **75** 141-54
- Grochulski W, Mitraszewski P and Penczek P 1985 Application of combined median averaging filters to scintigraphic image processing *Nucl. Med.* **24** 164-8
- Hawman E G 1981 Digital boundary techniques for the analysis of gated cardiac scintigrams *Opt. Eng.* **20** 719-25
- Hon T C, Rangayyan R M, Hahn L J and Kloiber R 1989 Restoration of gamma camera-based nuclear medicine images *IEEE Trans. Med. Imaging* **8** 354-63
- King M A, Doherty P M, Schwinger R B and Penney B C 1983 A Weiner filter for nuclear medicine images *Med. Phys.* **10** 876-80
- Miller T R, Goldman K J, Epstein D M and Biello D R 1984 Improved interpretation of gated cardiac images by use of digital filters *Radiology* **152** 795-800
- Pratt W K 1991 *Digital Image Processing* (New York: Wiley-Interscience) p 357
- Puchal R 1988 Restauración variante de imágenes en medicina nuclear *PhD Thesis* University of Barcelona p 83
- Reiber J H C, Lie S P, Simoons M L 1983 Clinical validation of fully automated computation of ejection fraction from gated equilibrium blood pool scintigrams *J. Nucl. Med.* **24** 1099-1107
- Schmitt M and Preteux F 1986 A new mathematical morphological algorithm: r, h maxima and r, h minima applications to x ray tomographs, NMR and angiography *Proc. Int. Electron. Image Week (Nice)* pp 470-75
- Serra J 1986 Introduction to mathematical morphology *Comput. Vision, Graphics Image Process.* **35** 283-305
- Stenberg S R 1986 Grayscale morphology *Comput. Vision, Graphics Image Process.* **35** 333-55